In situ characterisation of graphene growth on liquid copper-gallium alloys: Paving the path for cost-effective synthesis

Valentina Rein, Florian Letellier, Maciej Jankowski, Marc de Voogd, Mahesh Prabhu, Lipeng Yao, Gertjan van Baarle, Gilles Renaud, Mehdi Saedi, Irene M.N. Groot, et al.

Applied Surface Science 657 (2024) 159723

Contents lists available at ScienceDirect

Applied Surface Science

journal homepage: www.elsevier.com/locate/apsusc

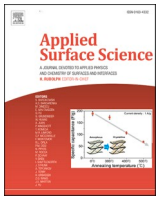

Full Length Article

In situ characterisation of graphene growth on liquid copper-gallium alloys: Paving the path for cost-effective synthesis

Valentina Rein [a,*], Florian Letellier [a], Maciej Jankowski [a], Marc de Voogd [b], Mahesh Prabhu [c], Lipeng Yao [a], Gertjan van Baarle [b], Gilles Renaud [d], Mehdi Saedi [e], Irene M.N. Groot [c], Oleg V. Konovalov [a,*]

[a] European Synchrotron Radiation Facility - ESRF, 71 Avenue des Martyrs, 38043 Grenoble, France
[b] Leiden Probe Microscopy (LPM), Kenauweg 21, 2331 BA Leiden, the Netherlands
[c] Leiden Institute of Chemistry, Leiden University, P.O. Box 9502, 2300 RA Leiden, the Netherlands
[d] Univ. Grenoble Alpes and CEA, IRIG/MEM/NRS, 38000 Grenoble, France
[e] Physics Department, Shahid Beheshti University, 1983969411 Tehran, Iran

ARTICLE INFO

Keywords:
Graphene
Liquid metal catalysts
Gallium
Chemical vapour deposition
Radiation-mode optical microscopy
X-ray reflectivity

ABSTRACT

Liquid metal catalysts (LMCats), primarily molten copper, have demonstrated their efficiency in the chemical vapour deposition (CVD) approach for synthesising highquality, large-area graphene. However, their high melting temperatures limit broader applications. Reducing the temperature of graphene production on LMCats would lead to a more efficient and cost-effective process. Here, we investigated the effects of alloying copper with a low-melting temperature metal on graphene growth in real-time. We examined a set of liquid copper-gallium alloy systems using two complementary *in situ* techniques: radiation-mode optical microscopy and synchrotron X-ray reflectivity (XRR). The microscopy observations revealed reduced catalytic activity and graphene quality degradation in compositions with gallium domination. The XRR confirmed the formation of single-layer graphene on alloys with up to 60 wt% of gallium. Furthermore, we detected a systematic increase in adsorption height on the alloys' surface, indicating weaker adhesion of graphene on gallium. These findings suggest that a trade-off between layer quality and cost reduction in production is feasible. Our results provide insights into the CVD synthesis of graphene on bimetallic liquid surfaces and underscore the potential of gallium-copper alloys for enabling the direct transfer of graphene from a liquid substrate, thereby addressing the limitations imposed by the high melting temperatures of conventional LMCats.

1. Introduction

The unique properties and versatility of two-dimensional materials (2DMs) such as graphene, germanene, h-BN, transition metal dichalcogenides, and others, along with their potential for industrial production, make them an exciting area of research with significant potential for technological advancement [1,2]. Graphene, which was first isolated in 2004, has become the benchmark of the 2DM family [3]. Since then, extensive studies have contributed to a deep understanding of graphene's unique properties, including high mechanical strength, electrical conductivity, thermal conductivity, flexibility, and transparency [4]. However, these promising properties of graphene are largely determined by its quality, which is defined by its crystallinity and defect density.

Over the years, the technology development of high-quality graphene production on a large scale has been an active area of research. The standard method for synthesising large-area graphene is chemical vapour deposition (CVD), which is commonly based on the catalytic decomposition of a hydrocarbon precursor gas on a solid metal substrate [5]. Based on experimental evidence, copper is considered the most effective substrate for graphene growth. The low solubility of carbon in Cu enables the growth of single-layer graphene over large areas [6–8]. Despite its wide application, several shortcomings generally associated with CVD on a solid substrate significantly compromise the quality of the graphene produced [9]. The solid substrate induces defects such as grain boundaries, vacancies, and lattice distortions. The growth rate and uniformity of the graphene sheet are difficult to control, leading to variations in its thickness and quality across the substrate. Only a few

* Corresponding authors.
E-mail addresses: valentina.belova@esrf.fr (V. Rein), konovalo@esrf.fr (O.V. Konovalov).

https://doi.org/10.1016/j.apsusc.2024.159723
Received 4 December 2023; Received in revised form 11 February 2024; Accepted 15 February 2024
Available online 17 February 2024

studies have reported the successful growth of large-area, fold-free monolayer graphene. It is important to mention that they used rather specific conditions, such as the conversion of commercial polycrystalline foils into monocrystalline Cu(1 1 1) foils, through annealing with a controlled temperature gradient, the use of ethylene as the precursor, and low growth temperatures resulting in low growth rates and high nucleation densities [7,8]. Successful attempts at direct deposition of ultra-flat graphene on a quartz substrate required elevated temperatures and strict control of contaminating particles [10]. Transferring the graphene layer from the solid substrate to another support inflicts further layer degradation. Ongoing research is focused on improving the scalability, yield, and quality of CVD-fabricated graphene. Developing new techniques to overcome the limitations of this method is crucial for the advanced applications and commercialisation of graphene and other 2DMs in highly demanding domains, such as micro- and nanotechnology.

The groundbreaking idea to replace solid metal catalysts with their liquid counterparts (LMCats) was first proposed by Wu *et al.* [11]. This approach yields high-quality, large-area single-crystal 2DMs with fewer defects and impurities [12,13]. LMCat substrates, such as liquid Cu, have atomically smooth surfaces, resulting in a low density of nucleation centres and fast mass transport. This allows for high growth rates that significantly reduce the density of defects and domain boundaries [14,15]. Direct deposition of graphene onto dielectric substrates, such as molten glass, has also been reported [16]. However, studies of LMCat-based CVD systems typically required cooling to room temperature, thus resolidifying the substrate and significantly altering the grown graphene. Furthermore, detailed information about the growth dynamics remained unknown.

Recently, we developed a customised CVD reactor, adapted to harsh conditions of CVD on LMCats, *e.g.* liquid Cu: a temperature of ~ 1400 K, a pressure of 200 mbar including CVD gas precursors, and intense metal evaporation. The reactor allows for X-ray reflectivity (XRR) and other X-ray scattering techniques, Raman spectroscopy, and radiation-mode optical microscopy to be combined for *in situ* characterisation in real-time during the growth [17]. The setup enables precise monitoring and control of graphene growth on liquid Cu in real time with high reproducibility [14,15]. The high quality of the synthesised graphene was confirmed through Raman characterisation.

Solidification of the liquid substrate would lead to deterioration in the quality of the graphene as produced. Therefore, the ultimate goal is a direct separation of continuously produced graphene with virtually infinite length from the hot liquid substrate, followed by its transfer to the target substrate without interruption. This concept was previously discussed in [17]. The successful development of such a direct separation method will largely depend on the physical and chemical interactions between the graphene layer and the LMCat, such as adsorption energy, catalytic activity, wettability, as well as the mechanical stability of the layer. Metal-graphene interactions are the crucial parameter in determining the most feasible transfer method for separating the graphene layer from the substrate [18]. Getting insight into these interactions demands understanding the interface's structure and proper modelling, which is well-established for solids [19–22] and supported by some experimental examples [23–26] but very scarce for liquid surfaces [27]. Additionally, the fracture strength of graphene is predicted to decrease with a rise in temperature [28]. Moreover, at high temperatures, separated graphene is at an increased risk of reacting with hydrogen or gas impurities (*e.g.* oxygen) [29,30]. Therefore, using low-melting-point LMCats to reduce the transfer process temperature without solidifying the substrate is advantageous. The low melting temperature pure metals Ga, In, and Sn have been previously reported in the literature as liquid catalysts for graphene CVD growth [31–34]. Moreover, using liquid Ga ($T_m = 303$ K), Lu *et al.* [35] demonstrated the possibility of a controllable sliding transfer of wafer-size graphene. However, the samples were characterised *ex-situ* and after solidification, leaving the detailed mechanisms of graphene formation largely unexplored. Given gallium's low melting point and its low adhesion energy with graphene [36], we consider it to be among the most promising LMCats for developing direct transfer technologies.

In addition, using lower temperatures during graphene growth will reduce energy consumption. Besides obvious economic benefits, it will simplify designing and operating the reactor for 2DM synthesis and separation. However, synthesising graphene at lower temperatures may also impede its growth rate and increase the number of defects. Hence, the conditions for graphene growth on Ga, which would allow a reasonable compromise between quality and gain in process temperature reduction, should be investigated. To this end, alloys of Cu and a metal with a low melting point have been successfully employed. For instance, introducing a CuSn alloy resulted in a reduction of the growth temperature of Mo_2C to some extent without compromising the growth rate or quality [37]. Alloying Cu with Zn allowed a slight temperature reduction and improved graphene quality (larger domain sizes and lower nucleation density) [38]. Here, we choose to study *in situ* the growth of graphene on liquid Ga and CuGa alloys of different compositions and, thus, melting points. A range of CuGa samples with varying compositions enables a gradual transition from the well-studied copper system to the novel gallium system. Comparing the results with those from Cu is essential in defining the most efficient growth process. The results obtained and the technical experience gained will aid in investigating the direct separation process using low-melting-point LMCats.

We used the LMCat reactor [17] equipped with a quartz window port filled with flowing methane as a precursor in a mixture of argon and hydrogen. The substrate temperature T_s was varied between an upper value of 1463 K and the melting point T_m of the corresponding $Cu_{(100-x)}Ga_x$ alloy: ~1360, ~1300, ~1210, ~1140, ~1070, ~970, ~870, ~780, and ~ 300 K for Ga concentrations x (in wt%) of 0 % (pure Cu), 10 %, 20 %, 30 %, 40 %, 50 %, 60 %, 70 % alloys, and 100 % (pure Ga), respectively [39]. The composition at the liquid surface was verified by *in situ* grazing-incidence X-ray fluorescence (XRF) and post-growth scanning electron microscopy (SEM) with energy-dispersive X-ray analysis (EDX). The probed depth below the surface of the two techniques is a few nanometres and a few micrometres, respectively. Two complementary *in situ* methods were employed for characterisation: radiation-mode optical microscopy and XRR. In situ optical microscopy provides information on the nucleation, growth rate, movements, and interactions of 2DMs on LMCats, while XRR helps to characterise the structural properties of the grown layers.

2. Results and discussion

2.1. Radiation-mode optical microscopy

Our recent work explored the growth behaviour of graphene on liquid Cu [14,15]. The details on the experimental setup are provided in the Materials and Methods section and the Supporting Information (SI) (Fig. S1). Under our typical experimental conditions, the growth starts with nucleation and formation of separate flakes whose shapes vary between circular, hexagonal, and concave-dodecagonal depending on the partial pressures p of the CVD precursors CH_4 and H_2. Then, due to an interplay between repulsive and attractive forces, the flakes self-assemble in a hexagonal lattice, filling the remaining surface of the liquid metal pool, followed by their coalescence in the last growth stage. Before coalescing, flakes can reach millimetres in lateral size depending on the growth rates. The remarkably low defect density of these flakes was proven by Raman spectroscopy characterisation.

To investigate whether and how Ga modifies the growth mechanism (s) of graphene and the catalytic activity of the liquid substrate, we prepared a series of $Cu_{(100-x)}Ga_x$ alloy samples with varying Ga weight composition x from 10 % to 100 %. Microscopy images were obtained through the quartz window aperture above the sample due to the difference in thermal emissivity between the graphene layer and the liquid metal. The measured emissivity of CuGa alloys is higher than those of

the pure metals separately, as shown in the SI, Fig. S2. This results in a lower emissivity contrast between the graphene flakes and the substrate for these samples. Nevertheless, the method can reliably determine the number of carbon layers because the emissivity scales proportionally [14]. Thus, white areas indicate the presence of multilayers or 3D domain formation, while monolayer graphene appears as homogeneous grey areas.

In general, the formation of carbon structures was observed for the entire concentration range of CuGa alloys. Fig. 1 displays the optical microscopy images of the typical growth modes observed at different coverage stages during growth as a function of Ga composition. The corresponding video files of the growths are available online as Movies S1-S5. The growth mechanisms undergo significant transformations from pure Cu [14,15] to pure Ga. No drastic change in the growth mechanisms is observed after adding 10 % of Ga to pure Cu (Fig. 1a–c). However, the growth rates and average flake sizes are smaller. Mostly, only circular shapes are observed. Additionally, merging of the flakes is observed at earlier growth stages, leading to the formation of branch-like structures. This may indicate a disturbance in the balance of repulsion-attraction interdomain forces toward a more substantial attractive contribution.

Increasing the Ga content further leads to a decrease in flake sizes. As deduced from Fig. 1d–f, for the $Cu_{70}Ga_{30}$ sample, most flakes are smaller than the camera's resolution, which is a few micrometres. Consequently,

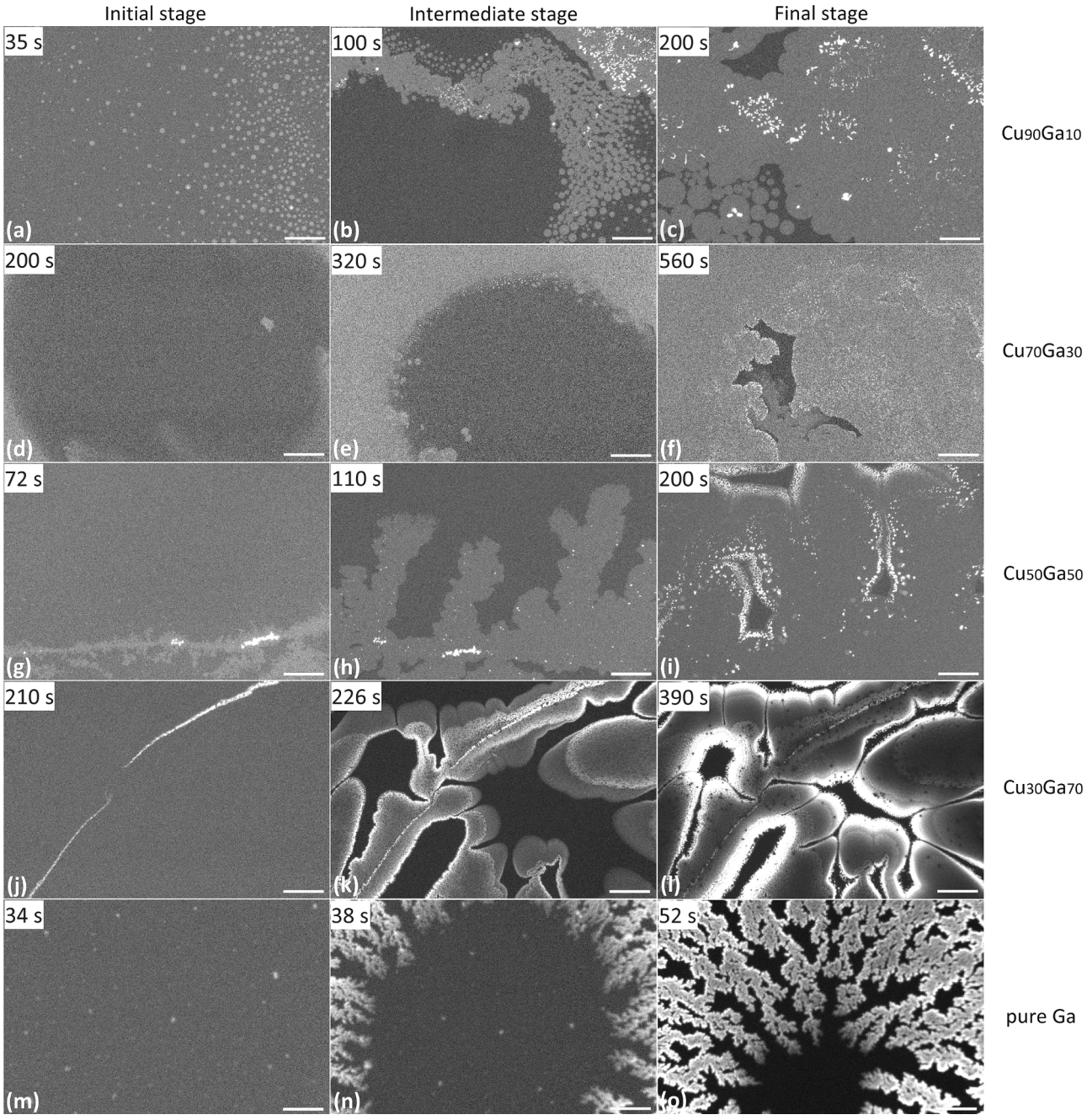

Fig. 1. Evolution of the growth mechanism of carbon layers on a liquid surface of CuGa alloys with an increase of Ga weight percentage from top to bottom. Different coverage stages are shown from left to right for the samples of 10 %, 30 %, 50 %, 70 %, and 100 % of Ga (the intermediate concentrations of 20 %, 40 %, and 60 % were also studied but omitted from the figure for clarity). The scale bar is 0.4 mm. The time is counted from the opening of the methane valve. The intensity scale corresponds to the emissivity ratio and is uniform across all images. The darkest shade of the grey scale corresponds to the liquid metal surface, with brightness increasing linearly with the number of carbon layers. The corresponding video files are available online as Movies S1-S5.

the assemblies of flakes appear as clouds due to a contrast gradient from the areas of highly concentrated flakes (light shade) to the clean alloy surface (dark shade). Graphene layer spreading can occur either through branch formation or flat front propagation from the sample edges towards the centre. Noteworthy, the growth slows down with higher coverage.

In samples with a higher percentage of Ga, it becomes impossible to distinguish single-crystal flakes. However, in the early stages, we can sometimes observe flakes of irregular shapes that seem to be clusters of graphene domains (Fig. 1g, m, n). As can be seen in the examples of 50 % (Fig. 1g–i), 70 % (Fig. 1j–l), and 100 % of Ga (Fig. 1m–o), the tendency towards anisotropic growth becomes stronger: the branches get narrower, giving rise to a more significant number of sprouts. Gallium also appears to facilitate the formation of multilayers and 3D structures, as evidenced by their high intensity on images due to the linear dependence of the emissivity on the number of carbon layers [14]. Consequently, we observe a noticeable shift in the growth pattern, from the formation of individual graphene crystals growing through isotropic 2D expansion, to the strongly anisotropic dendritic growth of carbon 3D structures. The change in layer quality can be traced by the increasing percentage of white areas, which are indicative of multilayers or 3D domains. It is worth noting that up to 60 % of Ga, the multilayers formed on top of graphene can be removed by etching with a CH_4/H_2 gas mixture for 10–40 min, resulting in a single layer (known as self-terminating growth) (refer to the SI, Fig. S3). However, the graphitic structures formed on the 70 % and 100 % Ga alloys are highly resistant to etching, and we were unable to remove them.

We have also carried out *ex-situ* post-growth characterisation using Raman spectroscopy on the series of alloy samples after the experiments (refer to SI, Fig. S4). The results confirm the transition observed by *in situ* optical microscopy from single-layer to multilayer growth when the Ga content exceeds 60 %. The D peak, which indicates the presence of defects, appears at 60 % of Ga. Up to this value, no significant deterioration in graphene quality is observed.

The change in growth mode can be followed with higher precision on the samples with low Ga content (between 0 % and 20 %), where individual flakes can still be visually distinguished by the camera (for flake diameters above ~ 25 μm, this limit may vary with the emissivity contrast between the flakes and the metal surface, which decreases with increasing Ga composition, see Fig. S2). Using a self-written MATLAB-based script for image analysis, we collected the statistics at the early/intermediate growth stages of the samples prior to flakes fusion, *i.e.* average flake size (diameter) and average number of visible flakes, shown in Fig. 2a,b (plots with data points for further values of p and T_s can be found in the SI, Fig. S5, S6). Here, we consider the range of the partial pressure ratio $p_{CH4}/p_{H2} \leq 0.05$ since, above this value, the nucleation density on pure Cu becomes very high, and consequently, the completion of a graphene layer occurs within seconds, leaving no room for proper analysis.

The graphs illustrate the typical behaviour of graphene flakes on pure Cu (0 % of Ga) under our standard experimental conditions. The nucleation density decreases as the substrate temperature T_s increases, but increases rapidly with the methane partial pressure p_{CH4}. This, in turn, correlates with a decrease in the average flake size as the available surface of the metal catalyst is covered faster, and the flakes have less time to grow before coalescing. For the 10 % and 20 % alloys, the general trend is a decrease in the average flake size. The number of visible flakes increases with the percentage of Ga at low methane partial pressure (square symbols) and decreases at higher p_{CH4}/p_{H2} (circle symbols). In addition, a decrease of T_s below ~ 1350 K (blue colour) promotes nucleation, while the average flake size follows a weak linear correlation with T_s. Remarkably, the apparent dependence of both parameters on the T_s and p diminishes as the Ga percentage increases to 20 wt%. In the $Cu_{80}Ga_{20}$ sample, most of the flakes nucleating at lower T_s have a size smaller than 25 μm and, therefore, cannot be included in the statistics. The decrease in flake size and increase in nucleation density is probably a consequence of the reduced mobility of carbon species on the surface of alloys [8,40].

The results of the analysis of the growth rates as a function of p_{CH4}/p_{H2} and T_s are shown in Fig. 2c, d. We see a notable decrease by more than one order of magnitude in the growth rates of the flakes (Fig. 2c) with the addition of 10 % and 20 % of Ga compared to pure Cu. For low Ga contents, where individual flakes are distinguishable, the growth rate is that of the average flake radius. For samples with a higher Ga content (≥30 %), we do not detect separate graphene flakes and instead use the growth rate of the edge of the growing graphene layer (Fig. 2d). Starting from the lowest Ga concentration considered in our study, $Cu_{90}Ga_{10}$, we observe a different growth mode: a continuous propagation of the layer

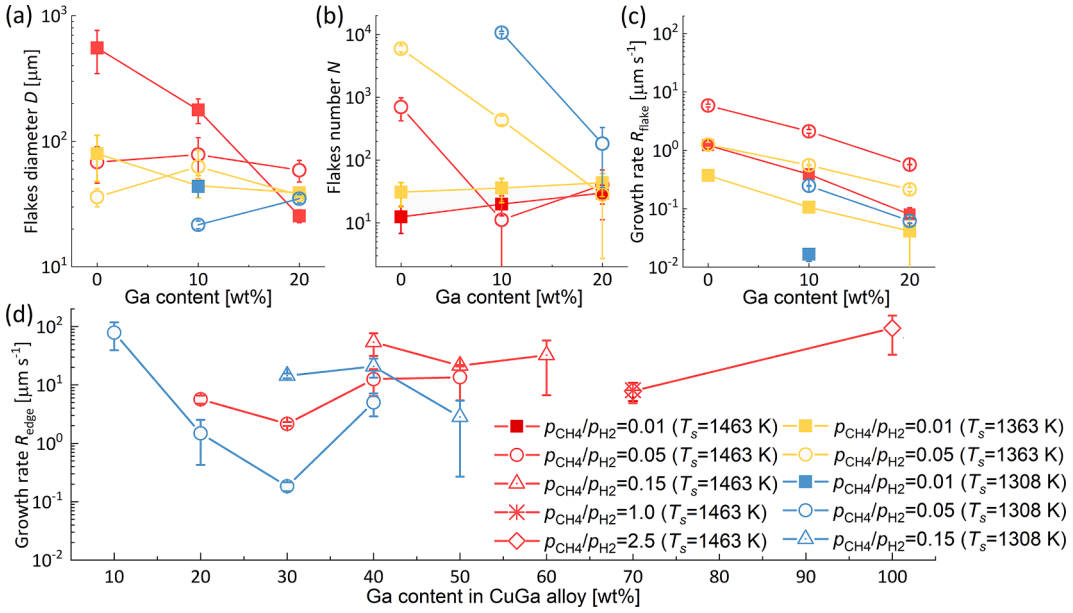

Fig. 2. Average flake diameter D (a) and average number of visible flakes N (b) observed within the field of view of the microscope at different T_s and p at early/intermediate growth stages (before merging) as a function of Ga percentage. Flake radius growth rate R_{flake} (c) and edge growth rate R_{edge} (d) at different p and T_s for the series of CuGa alloy compositions. Temperature colour code: red – 1463 K, yellow – 1363 K, blue – 1308 K. A log vertical scale is used for clarity.

from the LMCat edges at a relatively high rate (>20 μm s^{-1}). Counter-intuitively, this behaviour appears to be triggered by reducing T_s near or below the T_m of Cu (blue symbols in Fig. 2d). The same pattern of layer propagation at low T_s (below the Cu T_m of 1358 K) with rates that are higher than or equal to those at higher T_s (above the Cu T_m) is observed up to 50 % of Ga, although the rates decrease significantly below 1200 K (Fig. S6). For 20 % Ga, we see that the flake radius and edge growth rates are well-matched. Further increase in Ga concentration does not significantly affect the detectable growth rates. However, the p_{CH4}/p_{H2} threshold for graphene growth shifts towards larger values. Thus, transitioning from a 30 % sample to pure Ga, requires increasing p_{CH4} by two orders of magnitude to initiate and/or continue growth. Together with the reduced growth rates and layer quality, it corroborates the substantial decrease in the catalytic activity of Cu upon alloying with Ga and the inferior catalytic activity of Ga with respect to Cu. The differences in the growth and transport of C species may be attributed to the high carbon solubility within an ultra-thin surface layer of Ga assumed by Ueki *et al.* [41].

2.2. X-ray reflectivity

Using synchrotron XRR, we performed an *in situ* study of graphene layers grown *via* CVD on liquid CuGa alloys. XRR were recorded curves on the clean liquid alloy surfaces before and after the graphene growth. The reflectivity data from the curved liquid surfaces were treated according to the procedure described in Ref. [42]. Due to the sample curvature, the beam footprint on the surface varies between hundreds of microns, providing sufficient areal averaging [43]. The resulting curves are presented (open symbols) in Fig. 3a along with the fit (red solid lines), which aims to extract layers' roughness, thickness, and electron density profiles. The results of the fit, summarised in Table 1, are discussed further below.

As demonstrated in the previous section, the addition of a small quantity of Ga does not drastically alter the growth mechanism. The XRR curves of graphene layers on alloys containing up to 60 wt% of Ga closely resemble that of graphene on pure Cu (the upper curve), which has been proven to be of excellent quality [14]. The presence of only two Kiessig oscillations in the measured range, with a pronounced minimum for the scattering vector q_z in the range of 0.7–0.9 $Å^{-1}$ and the absence of a Bragg peak are clear signatures of single-layer graphene [44]. Additionally, the low roughness of only 1.12–1.63 Å is evidence of the reasonably good quality of the grown layers.

For the 70 % and 100 % Ga samples, the presence of a peak around 1.8 $Å^{-1}$, which is close to the (002) Bragg peak of graphite, is in agreement with the change in growth mode above 60 wt% of Ga to dendritic and 3D growth [45]. Note that, at variance with single-layer graphene, these multilayers could not be etched by increasing the H_2/CH_4 partial pressure ratio. The difficulty in achieving the growth of

Table 1
XRR fit results: the roughness of the liquid metal surface σ_m, the roughness of the carbon layer σ_C, and the thickness of the separation void t_v. The error bars in the last three columns result from the fitting procedure.

Nominal Ga content, wt%	Estimated actual Ga content, wt%*	σ_m, Å	σ_C, Å	t_v, Å
0	0	1.099 ± 0.008	1.119 ± 0.004	1.471 ± 0.007
10	9.5 ± 1.0	1.091 ± 0.013	1.178 ± 0.010	1.509 ± 0.017
20	17.5 ± 2.0	1.009 ± 0.019	1.194 ± 0.022	1.575 ± 0.028
30	25.4 ± 3.0	0.838 ± 0.028	1.162 ± 0.015	1.622 ± 0.022
40	36.0 ± 4.0	1.432 ± 0.024	1.422 ± 0.014	1.823 ± 0.024
50	39.0 ± 5.0	1.224 ± 0.008	1.599 ± 0.010	1.804 ± 0.008
60	56.0 ± 6.0	1.510 ± 0.015	1.626 ± 0.011	2.007 ± 0.016
70	65.0 ± 7.0	0.904 ± 0.050	2.076 ± 0.080	2.285 ± 0.124

* at the moment of scanning.

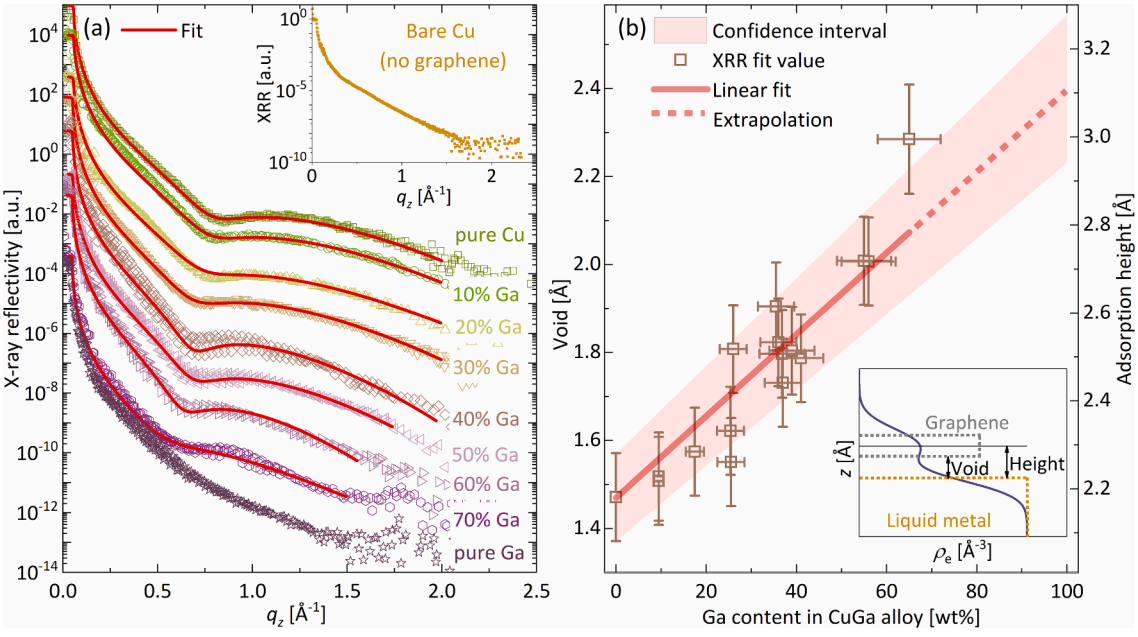

Fig. 3. (a) XRR curves of liquid CuGa alloy samples with CVD-grown graphene/graphite on top and the fit based on a slab model. The curves are vertically offset for clarity. The inset displays the XRR curve of bare liquid metal. (b) Graphene-copper adsorption height extracted from the fit of the XRR curves (void between Cu and C slabs plus half of the C slab, 0.71 Å). Single-layer graphene could not be observed and measured on pure Ga; therefore, no height value is reported. The inset illustrates the '*void*' and '*height*' definitions. The actual alloy compositions deviate from the nominal values due to an intense Ga evaporation in the liquid state. As a result, the horizontal error bar increases with the Ga contribution. The vertical error bar of 0.10 Å is based on the experimental reproducibility throughout the previous studies. The linear fit with a slope of 0.0093 ± 0.0007 Å/% demonstrates the linear relationship between the graphene-metal distance and the content of Ga. The confidence interval is a combination of these two uncertainties.

single-layer graphene on pristine Ga does not come as a surprise and may be attributed to variations in experimental conditions compared to previous attempts reported in the literature. On the one hand, gallium's ability to facilitate the formation of multilayer graphene and graphitic structures was observed previously [33,34,41,46–48]. On the other hand, previous reports on graphene CVD growth on liquid Ga did not involve the use of H_2. Consequently, a recent theoretical work [49] has raised doubts about previous results regarding graphene grown on Ga. The work suggests that the reported attempts, including the successful sliding transfer [31–35], were likely conducted under a residual pressure of O_2, which typically reacts with the Ga surface to form an oxide skin under the described conditions. Our observations also confirm that removing the oxide layer from liquid Ga requires high-temperature etching in an H_2 atmosphere. Since, in our experiment, the oxide layer was etched prior to carbon deposition, and H_2 flowed constantly during the CVD process, we can confidently rule out the aforementioned side effect. The presence or absence of oxide between graphene and gallium can significantly alter the adhesion force, and we, therefore, avoid direct comparison with previous reports, such as [35].

Another interesting observation in the XRR curves is a gradual shift of the first Kiessig minimum towards low q_z with increasing Ga content. We used the Refl1d software to fit the XRR curves [50], applying a slab model consisting of three slabs: Cu, C, and a separation void in between. The densities of liquid Cu and liquid Ga were taken from the literature [51,52]. The corresponding free parameters of the fits are summarised in Table 1. We recorded multiple scans for some compositions, the analysis of which can be found in the SI, Table S1. The void thickness corresponds directly to an important parameter, the interlayer graphene-copper distance, typically attributed to van der Waals interaction, which is also referred to as '*adsorption height*' [27]. In previous works, we defined this parameter as the distance between the inflection point of the Cu electron density ρ_e profile at the interface and the centre of the carbon slab [14,27,42,43]. Thus, the height is composed of the thickness of the void and half of the graphene layer thickness (1.42/2 Å). The height values obtained by fitting the XRR curves for the series of CuGa samples are shown in Fig. 3b, where we can observe a systematic increase with increasing Ga percentage. We note that the *in situ* grazing-incidence XRF analysis, which is surface sensitive, did not reveal any significant deviation from the nominal composition ratio at the liquid surface during the experiments (see Fig. S7 in the SI). However, due to intense metal evaporation, the content of the CuGa samples shifted towards a lower Ga contribution, according to post-growth SEM-EDX (see the SI for more details, Tables S2, S3, and Fig. S8). Based on the EDX results, we estimate the content during each XRR measurement by assuming that the Ga loss is linear with time and set the uncertainty as 10 % of the nominal Ga percentage (see Table 1). We apply an error bar of 0.10 Å for the height values based on the experimental reproducibility according to our previous works [14,27,42,43]. Assuming a linear dependence of the distance on Ga concentration (the slope resulting from the linear fit is 0.0093 ± 0.0007 Å/%), the extrapolation suggests an increase from 2.18 ± 0.10 Å on liquid Cu to 3.11 ± 0.17 Å on liquid Ga. To estimate the confidence interval, we combine the error bar of the starting point of 0.10 Å and the fit uncertainty for the slope.

Qualitatively, the value of the adsorption height allows for estimating the strength of the graphene-metal bonding and the work needed to separate the graphene from its substrate, *e.g.*, to transfer it to another substrate. This trend has been well-documented for solid, crystalline, and transition metal substrates. Strong bonding, *e.g.*, with Co, Ni, Ru, Rh, and Re, typically corresponds to graphene-metal distances of ~ 2.1 Å. In contrast, weak bonding (*e.g.*, with Cu, Ag, Al, Ir, Pt, and Au) corresponds to more than 1 Å larger distances of ~ 3–3.4 Å, typical of weak van der Waals bonding (close to the interlayer distance of 3.35 Å in bulk graphite) [22]. In a first rough approximation [53], the bonding of graphene with metals is primarily due to the metal d-band electrons. Indeed, Batzill *et al.* [53] observed that the metal-graphene distance increases when the distance between the *d*-band and the Fermi level increases. Thus, we expect that the metal distance increase from Co to Ni, then to Cu, and shall continue to increase for the following metals, Zn and Ga. Note that, strictly speaking, Zn and Ga are not transition metals since their 3*d* band is filled, unlike Cu. However, we can expect that the further filling of the 4 *s* and 4*p* bands will only further weaken the bond strength. Another factor along this trend could be the larger van der Waals radius of Ga (1.87 Å) compared to Cu (1.40 Å). Additionally, Ga can be considered electronically similar to Al, which is located in the same column (13th) of the periodic table of elements. The graphene–to–Al distance is the greatest reported (3.41 Å).

3. Conclusion

In summary, this study investigates the effect of copper-gallium alloying on the growth of graphene and assesses the potential of CuGa alloys as a liquid catalyst for cost-effective graphene synthesis by CVD. It is done by combining *in situ* radiation-mode optical microscopy and XRR to track the growth mode of graphene on the liquid substrate in real time. We find that the alloying of Cu with Ga drastically alters the growth mechanism of graphene. The catalytic activity of the liquid substrate appears to decline, and the grown material undergoes a transition from large discrete flakes at minor Ga content to continuous growth with an increase in concentration, which then evolves into slow branched 3D growth as Ga dominates. This transformation also corresponds to irreversible alterations in graphene quality, as the multilayer/3D structures cannot be removed by etching on alloys with high Ga content (above 60 %). The XRR data indicates the formation of single-layer graphene up to 60 wt% of Ga. At this concentration, the melting point decreases to ~ 873 K compared to 1358 K of pure Cu. Furthermore, the gradual shift of the first Kiessig minimum in the direction of low q_z with increasing Ga content points toward a somewhat weaker van der Waals interaction between graphene and gallium in comparison to copper.

The findings of this study provide offer into graphene synthesis and highlight the potential of CuGa alloys to serve as liquid metal catalysts with a weaker adhesion to graphene and a melting temperature reduced by a few hundred degrees as a replacement for high-melting temperature copper. Furthermore, this is achieved while maintaining a decent catalytic activity and the quality of the grown graphene in the case of the alloys with medium Ga content. The observations reported here are expected to facilitate the development of technologies for the direct separation of graphene from liquid substrates without solidification and degradation of the quality of the grown layer. As a result, our research has significant potential for implications in the production technologies and commercialisation of graphene and other 2DMs. The experimentally obtained parameters are also of great interest for theoretical studies, particularly in the domain of molecular simulations, where experimental input is often lacking.

4. Materials and methods

In order to investigate the catalytic activity of liquid Ga for CVD graphene growth compared to liquid Cu, we prepared a series of CuGa alloys with varying content of Ga from 10 wt% to pure Ga. The Cu foils, 50 µm thick and of 99.9976 % purity, were purchased from Advent Research Materials (Eynsham, The United Kingdom). The Ga lump of 99.9999 % purity was purchased from Goodfellow (Lille, France). The alloy samples were prepared by melting Cu and Ga pieces (a small shot of Ga placed on top of the foils) on a tungsten disk, used as a sample holder, inside the reactor prior to the experiments. The weight of each component was controlled by a microbalance (accuracy of 10 µg). The tungsten disks with a diameter of 25 mm were purchased from Metel BV (Waalwijk, The Netherlands). The percentage of Ga at the beginning of each growth experiment was verified by the decrease of the alloy's melting/solidification point T_m compared to pristine Cu according to the known phase diagram [39]. For selected compositions, we checked the

ratio at the surface (within a probed depth of a few nm) with *in situ* grazing-incidence XRF. The final bulk composition was estimated on the solidified alloys by SEM-EDX measurements, as reported in Table S2 and further discussed in the SI. The mobile CVD reactor with the attached gas system was specifically designed for *in situ* optical and X-ray measurements of graphene growth at high temperatures above that of liquid Cu [17] (see also Fig. S1). The growth process was monitored and recorded using optical microscopy in the radiation mode with a × 5 objective and a digital camera. The flakes and layers of graphene can be visually distinguished from bare Cu surface due to their higher emissivity, which results in higher intensity contrast. Moreover, the brightness scales linearly with the number of carbon layers [14]. The experimental range of T_s was limited by the solidification point of the alloys on the lower side to a maximum of 1473 K restricted by the heater power and safety. A standard set of gases purchased from Air Liquide (Paris, France) was employed: Ar, H_2, and CH_4. The methane gas was delivered in bottles of two concentrations: 5 % diluted in Ar and 100 %. The flowmeters built into the gas system controlled the partial pressure ratio of CH_4 to H_2 and varied between 0 and 2.5.

The experimental conditions for the growths shown in Fig. 1 in the main text and online video files Movies S1–S5 were:

$Cu_{90}Ga_{10}$ (Movie S1): $T_s = 1413$ K, $P_{CH4}/P_{H2} = 4.4 \times 10^{-2}$.
$Cu_{70}Ga_{30}$ (Movie S2): $T_s = 1308$ K, $P_{CH4}/P_{H2} = 1.3 \times 10^{-1}$-$1.9 \times 10^{-1}$.
$Cu_{50}Ga_{50}$ (Movie S3): $T_s = 1463$ K, $P_{CH4}/P_{H2} = 4.4 \times 10^{-2}$-$1.3 \times 10^{-1}$.
$Cu_{30}Ga_{70}$ (Movie S4): $T_s = 1463$ K, $P_{CH4}/P_{H2} = 1.0$–2.5.
Ga_{100} (Movie S5): $T_s = 1463$ K, $P_{CH4}/P_{H2} = 2.5$.

The X-ray study was carried out at beamline ID10 of the European Synchrotron Radiation Facilities (ESRF, France). The beamline is equipped with a double-crystal deflector that enables the definition and variation of the incident angle of the X-ray beam with respect to liquid surfaces while keeping them horizontal [54]. The beam energy was set to 22 keV, and its size did not exceed 15 μm in the vertical and horizontal directions. The data were acquired with a 2D MAXIPIX detector using CdTe pixels. The reflectivity data obtained from the curved liquid surfaces were processed according to the procedure described by Konovalov *et al.* [42].

Author Contributions

The manuscript was written through the contributions of all authors. All authors approved the final version of the manuscript.

Data availability

The X-ray data collected during the beamtime experiment MA-5338 at the ID10 beamline of the ESRF is available at https://data.esrf.fr/doi/https://doi.org/10.15151/ESRF-ES-787695481. The microscopy data can be provided upon reasonable request.

CRediT authorship contribution statement

Valentina Rein: Writing – original draft, Visualization, Investigation, Formal analysis, Conceptualization. **Florian Letellier:** Investigation. **Maciej Jankowski:** Writing – review & editing, Software, Methodology, Investigation, Data curation, Conceptualization. **Marc de Voogd:** Investigation. **Mahesh Prabhu:** Investigation. **Lipeng Yao:** Investigation. **Gertjan van Baarle:** Supervision, Methodology. **Gilles Renaud:** Writing – review & editing, Conceptualization. **Mehdi Saedi:** Writing – review & editing, Methodology, Funding acquisition, Conceptualization. **Irene M.N. Groot:** Writing – review & editing, Project administration, Funding acquisition. **Oleg V. Konovalov:** Writing – review & editing, Supervision, Investigation.

Declaration of competing interest

The authors declare the following financial interests/personal relationships which may be considered as potential competing interests: Valentin Rein reports financial support was provided by Horizon 2020 Framework Programme. If there are other authors, they declare that they have no known competing financial interests or personal relationships that could have appeared to influence the work reported in this paper.

Data availability

Data will be made available on request.

Acknowledgements

The authors express their gratitude to the European Synchrotron Radiation Facility for providing access to the synchrotron radiation facilities and for allowing the use of the surface scattering end-station at beamline ID10. We are grateful to Irina Snigireva (ESRF, Grenoble) for assistance with the SEM EDX measurements. Additionally, the authors acknowledge the financial support provided by Grant Agreement No. 951943 (DirectSepa) from the European Union's Horizon 2020 research and innovation program.

Appendix A. Supplementary material

Supplementary data to this article (schematic of the CVD reactor, alloys' emissivity, etching effect, *ex-situ* Raman spectra, plots with quantitative characterisation with microscopy, extended table of the XRR fit parameters, alloy composition determination with XRF and SEM EDX, and movies of the growths).

Supplementary data to this article can be found online at https://doi.org/10.1016/j.apsusc.2024.159723.

References

[1] A. Gupta, T. Sakthivel, S. Seal, Recent development in 2D materials beyond graphene, Prog. Mater. Sci. 73 (2015) 44–126, https://doi.org/10.1016/j.pmatsci.2015.02.002.
[2] P. Ares, K.S. Novoselov, Recent advances in graphene and other 2D materials, Nano Mater. Sci. 4 (2022) 3–9, https://doi.org/10.1016/j.nanoms.2021.05.002.
[3] K.S. Novoselov, A.K. Geim, S.V. Morozov, D. Jiang, Y. Zhang, S.V. Dubonos, I. V. Grigorieva, A.A. Firsov, Electric field effect in atomically thin carbon films, Science. 306 (2004) 666–669, https://doi.org/10.1126/science.1102896.
[4] S.K. Tiwari, R.K. Mishra, S.K. Ha, A. Huczko, Evolution of graphene oxide and graphene: from imagination to industrialisation, ChemNanoMat. 4 (2018) 598–620, https://doi.org/10.1002/cnma.201800089.
[5] K. Jia, J. Zhang, Y. Zhu, L. Sun, L. Lin, Z. Liu, Toward the commercialisation of chemical vapor deposition graphene films, Appl. Phys. Rev. 8 (2021) 041306, https://doi.org/10.1063/5.0056413.
[6] X. Li, W. Cai, L. Colombo, R.S. Ruoff, Evolution of graphene growth on Ni and Cu by carbon isotope labeling, Nano Lett. 9 (2009) 4268–4272, https://doi.org/10.1021/nl902515k.
[7] L. Sun, B. Chen, W. Wang, Y. Li, X. Zeng, H. Liu, Y. Liang, Z. Zhao, A. Cai, R. Zhang, Y. Zhu, Y. Wang, Y. Song, Q. Ding, X. Gao, H. Peng, Z. Li, L. Lin, Z. Liu, Toward Epitaxial Growth of Misorientation-Free Graphene on Cu(111) Foils, ACS Nano. 16 (2022) 285–294, https://doi.org/10.1021/acsnano.1c06285.
[8] M. Wang, M. Huang, D. Luo, Y. Li1, M. Choe, W.K. Seong, M. Kim, S. Jin, M. Wang, S. Chatterjee, Y. Kwon, Z. Lee, R.S. Ruof, Single-crystal, large-area, fold-free monolayer graphene, Nature. 596 (2021) 519-524. doi:10.1038/s41586-021-03753-3.
[9] L. Lin, B. Deng, J. Sun, H. Peng, Z. Liu, Bridging the gap between reality and ideal in chemical vapor deposition growth of graphene, Chem. Rev. 118 (2018) 9281–9343, https://doi.org/10.1021/acs.chemrev.8b00325.
[10] B. Jiang, D. Liang, Z. Sun, H. Ci, B. Liu, Y. Gao, J. Shan, X. Yang, M.H. Rümmeli, J. Wang, T. Wei, J. Sun, Z. Liu, Toward Direct Growth of Ultra-Flat Graphene, Adv. Funct. Mater. 32 (2022) 2200428, https://doi.org/10.1002/adfm.202200428.
[11] Y.A. Wu, Y. Fan, S. Speller, G.L. Creeth, J.T. Sadowski, K. He, A.W. Robertson, C. S. Allen, J.H. Warner, Large single crystals of graphene on melted copper using chemical vapor deposition, ACS Nano. 6 (2012) 5010–5017, https://doi.org/10.1021/nn3016629.
[12] J. Liu, L. Fu, Controllable growth of graphene on liquid surfaces, Adv. Mater. 31 (2019) 1800690, https://doi.org/10.1002/adma.201800690.

[13] C. Tsakonas, M. Dimitropoulos, A.C. Manikas, C. Galiotis, Growth and In situ characterisation of 2D materials by chemical vapour deposition on liquid metal catalysts: a review, Nanoscale. 13 (2021) 3346–3373, https://doi.org/10.1039/d0nr07330j.
[14] M. Jankowski, M. Saedi, F. La Porta, A.C. Manikas, C. Tsakonas, J.S. Cingolani, M. Andersen, M. De Voogd, G.J.C. Van Baarle, K. Reuter, C. Galiotis, G. Renaud, O. V. Konovalov, I.M.N. Groot, Real-time multiscale monitoring and tailoring of graphene growth on liquid copper, ACS Nano. 15 (2021) 9638–9648, https://doi.org/10.1021/acsnano.0c10377.
[15] V. Belova, H. Gao, H. Heenen, W. Sghaier, A. Manikas, M. Saedi, J.T. Margraf, C. Galiotis, G. Renaud, O. V Konovalov, I.M.N. Groot, K. Reuter, M. Jankowski, Operando Characterization and Machine-Learning Surrogated Molecular Simulations Reveal the Growth Kinetics of Graphene on Liquid Copper during Chemical Vapor Deposition, preprint (2023). doi:10.48550/arXiv.2305.18331.
[16] Y. Chen, J. Sun, J. Gao, F. Du, Q. Han, Y. Nie, Z. Chen, A. Bachmatiuk, M. Kr, D. Priydarshi, X. Ma, X. Song, C. Wu, M.H. Xiong, F. Rümmeli, Y. Ding, Z.L. Zhang, Growing Uniform Graphene Disks and Films on Molten Glass for Heating Devices and Cell Culture, Adv. Mater. 27 (2015) 7839–7846, https://doi.org/10.1002/adma.201504229.
[17] M. Saedi, J.M. De Voogd, A. Sjardin, A. Manikas, C. Galiotis, M. Jankowski, G. Renaud, F. La Porta, O. Konovalov, G.J.C. Van Baarle, I.M.N. Groot, Development of a reactor for the in situ monitoring of 2D materials growth on liquid metal catalysts, using synchrotron X-ray scattering, Raman spectroscopy, and optical microscopy, Rev. Sci. Instrum. 91 (2020) 013907, https://doi.org/10.1063/1.5110656.
[18] L.P. Ma, W. Ren, H.M. Cheng, Transfer methods of graphene from metal substrates: a review, Small Methods. 3 (2019) 1900049, https://doi.org/10.1002/smtd.201900049.
[19] P.A. Khomyakov, G. Giovannetti, P.C. Rusu, G. Brocks, J. Van Den Brink, P.J. Kelly, First-principles study of the interaction and charge transfer between graphene and metals, Phys. Rev. B - Condens. Matter Mater. Phys. 79 (2009) 195425, https://doi.org/10.1103/PhysRevB.79.195425.
[20] M. Vanin, J.J. Mortensen, A.K. Kelkkanen, J.M. Garcia-Lastra, K.S. Thygesen, K. W. Jacobsen, Graphene on metals: a van der Waals density functional study, Phys. Rev. B - Condens. Matter Mater. Phys. 81 (2010) 081408, https://doi.org/10.1103/PhysRevB.81.081408.
[21] B.J. Schultz, R.V. Dennis, V. Lee, S. Banerjee, An electronic structure perspective of graphene interfaces, Nanoscale. 6 (2014) 3444–3466, https://doi.org/10.1039/c3nr06923k.
[22] M. Yang, Y. Liu, T. Fan, D. Zhang, Metal-graphene interfaces in epitaxial and bulk systems: A review, Prog. Mater. Sci. 110 (2020) 100652, https://doi.org/10.1016/j.pmatsci.2020.100652.
[23] F. Jean, T. Zhou, N. Blanc, R. Felici, J. Coraux, G. Renaud, Topography of the graphene/Ir(111) moiré studied by surface x-ray diffraction, Phys. Rev. B - Condens. Matter Mater. Phys. 91 (2015) 245424, https://doi.org/10.1103/PhysRevB.91.245424.
[24] Y. Fukaya, S. Entani, S. Sakai, I. Mochizuki, K. Wada, T. Hyodo, S.I. Shamoto, Spacing between graphene and metal substrates studied with total-reflection high-energy positron diffraction, Carbon N. Y. 103 (2016) 1–4, https://doi.org/10.1016/j.carbon.2016.03.006.
[25] Y. Fukaya, A. Kawasuso, A. Ichimiya, T. Hyodo, Total-reflection high-energy positron diffraction (TRHEPD) for structure determination of the topmost and immediate sub-surface atomic layers, J. Phys. D. Appl. Phys. 52 (2019) 013002, https://doi.org/10.1088/1361-6463/aadf14.
[26] S. Entani, M. Honda, H. Naramoto, S. Li, S. Sakai, Synchrotron X-ray standing wave Characterisation of atomic arrangement at interface between transferred graphene and α-Al2O3(0001), Surf. Sci. 704 (2021) 121749, https://doi.org/10.1016/j.susc.2020.121749.
[27] H. Gao, V. Belova, F. La Porta, J.S. Cingolani, M. Andersen, M. Saedi, O. V. Konovalov, M. Jankowski, H.H. Heenen, I.M.N. Groot, G. Renaud, K. Reuter, Graphene at liquid copper catalysts: atomic-scale agreement of experimental and first-principles adsorption height, Adv. Sci. 9 (2022) 2204684, https://doi.org/10.1002/advs.202204684.
[28] H. Zhao, N.R. Aluru, Temperature and strain-rate dependent fracture strength of graphene, J. Appl. Phys. 108 (2010) 064321, https://doi.org/10.1063/1.3488620.
[29] Y. Zhang, Z. Li, P. Kim, L. Zhang, C. Zhou, Anisotropic hydrogen etching of chemical vapor deposited graphene, ACS Nano. 6 (2012) 126–132, https://doi.org/10.1021/nn202996r.
[30] A. Eftekhari, P. Jafarkhani, Curly graphene with specious interlayers displaying superior capacity for hydrogen storage, J. Phys. Chem. C. 117 (2013) 25845–25851, https://doi.org/10.1021/jp410044v.
[31] J.I. Fujita, Y. Miyazawa, R. Ueki, M. Sasaki, T. Saito, Fabrication of large-area graphene using liquid gallium and its electrical properties, Jpn. J. Appl. Phys. 49 (2010) 06GC01, https://doi.org/10.1143/JJAP.49.06GC01.
[32] G. Ding, Y. Zhu, S. Wang, Q. Gong, L. Sun, T. Wu, X. Xie, M. Jiang, Chemical vapor deposition of graphene on liquid metal catalysts, Carbon N. Y. 53 (2013) 321–326, https://doi.org/10.1016/j.carbon.2012.11.018.
[33] L. Gao, G.X. Ni, Y. Liu, B. Liu, A.H. Castro Neto, K.P. Loh, Face-to-face transfer of wafer-scale graphene films, Nature. 505 (2014) 190–194, https://doi.org/10.1038/nature12763.
[34] J.I. Fujita, T. Hiyama, A. Hirukawa, T. Kondo, J. Nakamura, S.I. Ito, R. Araki, Y. Ito, M. Takeguchi, W.W. Pai, Near room temperature chemical vapor deposition of graphene with diluted methane and molten gallium catalyst, Sci. Rep. 7 (2017) 12371, https://doi.org/10.1038/s41598-017-12380-w.
[35] W. Lu, M. Zeng, X. Li, J. Wang, L. Tan, M. Shao, J. Han, S. Wang, S. Yue, T. Zhang, X. Hu, R.G. Mendes, M.H. Rümmeli, L. Peng, Z. Liu, L. Fu, Controllable Sliding Transfer of Wafer-Size Graphene, Adv. Sci. 3 (2016) 1600006, https://doi.org/10.1002/advs.201600006.
[36] J.V. Naidich, J.N. Chuvashov, Wettability and contact interaction of gallium-containing melts with non-metallic solids, J. Mater. Sci. 18 (1983) 2071–2080, https://doi.org/10.1007/BF00555000.
[37] S. Chaitoglou, T. Giannakopoulou, T. Speliotis, A. Vavouliotis, C. Trapalis, A. Dimoulas, Mo_2C/graphene heterostructures: low temperature chemical vapor deposition on liquid bimetallic Sn–Cu and hydrogen evolution reaction electrocatalytic properties, Nanotechnology. 30 (2019) 125401, https://doi.org/10.1088/1361-6528/aaf9e8.
[38] L. Li, M. Li, R. Zhang, Q. Zhang, H. Li, D. Geng, Liquid Cu–Zn catalyzed growth of graphene single-crystals, New J. Chem. 47 (2023) 20703, https://doi.org/10.1039/d3nj03345g.
[39] H. Okamoto, Supplemental Literature Review of Binary Phase Diagrams: Al-Nd, Al-Sm, Al-V, Bi-Yb, Ca-In, Ca-Sb, Cr-Nb, Cu-Ga, Ge-O, Pt-Sn, Re-Y, and Te-Yb, J. Phase Equilibria Diffus. 37 (2016) 350–362, https://doi.org/10.1007/s11669-016-0452-4.
[40] H. Kim, C. Mattevi, M.R. Calvo, J.C. Oberg, L. Artiglia, S. Agnoli, C.F. Hirjibehedin, M. Chhowalla, E. Saiz, Activation Energy Paths for Graphene Nucleation and Growth on Cu, ACS Nano. 6 (2012) 3614–3623, https://doi.org/10.1021/nn3008965.
[41] R. Ueki, T. Nishijima, T. Hikata, S. Ookubo, R. Utsunomiya, T. Matsuba, J.I. Fujita, In-situ observation of surface graphitisation of gallium droplet and concentration of carbon in liquid gallium, Jpn. J. Appl. Phys. 51 (2012) 06FD28, https://doi.org/10.1143/JJAP.51.06FD28.
[42] O.V. Konovalov, V. Belova, F. La Porta, M. Saedi, I.M.N. Groot, G. Renaud, I. Snigireva, A. Snigirev, M. Voevodina, C. Shen, A. Sartori, B.M. Murphy, M. Jankowski, X-ray reflectivity from curved surfaces as illustrated by a graphene layer on molten copper, J. Synchrotron Radiat. 29 (2022) 711–720, https://doi.org/10.1107/s1600577522002053.
[43] V. Belova, M. Jankowski, M. Saedi, I.M.N. Groot, G. Renaud, O.V. Konovalov, Employing surface curvature for spatially resolved X-ray reflectivity: graphene domains on liquid copper, Adv. Mater. Interfaces. 10 (2023) 2300053, https://doi.org/10.1002/admi.202300053.
[44] H. Kiessig, Interferenz von Röntgenstrahlen an dünnen Schichten, Ann. Phys. 5 (1931) 769–788.
[45] J.Y. Howe, C.J. Rawn, L.E. Jones, H. Ow, Improved crystallographic data for graphite, Powder Diffr. 18 (2003) 150–154, https://doi.org/10.1154/1.1536926.
[46] J. Fujita, R. Ueki, Y. Miyazawa, T. Ichihashi, Graphitization at interface between amorphous carbon and liquid gallium for fabricating large area graphene sheets, J. Vac. Sci. Technol. B Microelectron. Nanom. Struct. 27 (2009) 3063, https://doi.org/10.1116/1.3253542.
[47] Z.W. Pan, S. Dai, D.B. Beach, N.D. Evans, D.H. Lowndes, Gallium-mediated growth of multiwall carbon nanotubes, Appl. Phys. Lett. 82 (2003) 1947–1949, https://doi.org/10.1063/1.1563727.
[48] A. Mukanova, R. Tussupbayev, A. Sabitov, I. Bondarenko, R. Nemkaeva, B. Aldamzharov, Z. Bakenov, CVD graphene growth on a surface of liquid gallium, Mater. Today Proc. 4 (2017) 4548–4554, https://doi.org/10.1016/j.matpr.2017.04.028.
[49] M. Saedi, S.M. Mohseni, I.M.N. Groot, Thermodynamic analysis of graphene CVD grown on liquid metal: Growth on liquid metallic gallium or solid gallium oxide skin? Mater. Chem. Phys. 275 (2022) 125203 https://doi.org/10.1016/j.matchemphys.2021.125203.
[50] P.A. Kienzle, J. Krycka, N. Patel, I. Sahin, Refl1D (Version 0.8.16), College Park, MD: University of Maryland, November 14, 2023. doi.org/10.5281/zenodo.4329338.
[51] M.J. Assael, A.E. Kalyva, K.D. Antoniadis, R. Michael Banish, I. Egry, J. Wu, E. Kaschnitz, W.A. Wakeham, Reference data for the density and viscosity of liquid copper and liquid tin, J. Phys. Chem. Ref. Data. 39 (2010) 033105, https://doi.org/10.1063/1.3467496.
[52] M.J. Assael, I.J. Armyra, J. Brillo, S.V. Stankus, J. Wu, W.A. Wakeham, Reference data for the density and viscosity of liquid cadmium, cobalt, gallium, indium, mercury, silicon, thallium, and zinc, J. Phys. Chem. Ref. Data. 41 (2012) 033101, https://doi.org/10.1063/1.4729873.
[53] M. Batzill, The surface science of graphene: Metal interfaces, CVD synthesis, nanoribbons, chemical modifications, and defects, Surf. Sci. Rep. 67 (2012) 83–115, https://doi.org/10.1016/j.surfrep.2011.12.001.
[54] O. Konovalov, V. Rein, M. Saedi, I. Groot, G. Renaud, M. Jankowski, Tripling of the scattering vector range of X-ray reflectivity on liquid surfaces using a double-crystal deflector, J. Appl. Cryst. 57 (2024), https://doi.org/10.1107/S1600576724000657.